J|A|C|S ARTICLES

Published on Web 11/17/2009

Size Effects in the $Li_{4+x}Ti_5O_{12}$ Spinel

W. J. H. Borghols,[†,‡] M. Wagemaker,[*,†] U. Lafont,[§] E. M. Kelder,[§] and F. M. Mulder[†]

Department of Radiation, Radionuclides and Reactors, Faculty of Applied Sciences, Delft University of Technology, Mekelweg 15, 2629 JB Delft, The Netherlands, Institut für Festkörperforschung, Jülich Centre for Neutron Science at FRM II, Forschungszentrum Jülich GmbH, Lichtenbergstrasse 1, 85747 Garching, Germany, and Delft Chem Tech, Faculty of Applied Sciences, Delft University of Technology, Julianalaan 136, 2628 BL Delft, The Netherlands

Received March 26, 2009; E-mail: m.wagemaker@tudelft.nl

Abstract: The nanosized $Li_{4+x}Ti_5O_{12}$ spinel is investigated by electrochemical (dis)charging and neutron diffraction. The near-surface environment of the nanosized particles allows higher Li ion occupancies, leading to a larger storage capacity. However, too high surface lithium storage leads to irreversible capacity loss, most likely due to surface reconstruction or mechanical failure. A mechanism where the large near-surface capacity ultimately leads to surface reconstruction rationalizes the existence of an optimal particle size. Recent literature attributes the curved voltage profiles, leading to a reduced length of the voltage plateau, of nanosized electrode particles to strain and interface energy from the coexisting end members. However, the unique zero-strain property of the $Li_{4+x}Ti_5O_{12}$ spinel implies a different origin of the curved voltage profiles observed for its nanosized crystallites. It is proposed to be the consequence of different structural environments in the near-surface region, depending on the distance from the surface and surface orientation, leading to a distribution of redox potentials in the near-surface area. This phenomenon may be expected to play a significant role in all nanoinsertion materials displaying the typical curved voltage curves with reduced length of the constant-voltage plateau.

Introduction

The $Li_4Ti_5O_{12}$ spinel is the end member of the solid solution region described by $Li_{3+y}Ti_{6-y}O_{12}$ ($0 \leq y \leq 1$).[1] At first, the spinels in this range drew attention due to the finding of superconductivity at relatively high transition temperatures.[2] In 1994, Ferg et al. first described the possible application of this compound as an electrode material in a secondary Li ion battery.[3] The disadvantage of having a high voltage of ~1.55 V versus Li metal compared to anode materials such as graphite is compensated by the material's safe operation, high rate capability, low cost, and excellent recyclability. The latter is attributed to the minimal decrease in unit cell volume of only 0.2% between both members $Li_4Ti_5O_{12}$ and $Li_7Ti_5O_{12}$, where the lattice axes change from 8.3595 Å[1] to 8.3538 Å,[4] respectively. In $Li_4Ti_5O_{12}$, abbreviated as LTO, all tetrahedral 8a sites are occupied by lithium, resulting in $(Li_3)_{8a}[Li_1Ti_5]_{16d}(O_{12})_{32e}$. Similar to the pure spinel ($y = 0$),[5] lithiation leads to 16c occupation and in addition causes Li ions to move from 8a toward 16c positions. This is most likely caused by the Coulomb repulsion between nearest Li ions occupying the 8a−16c positions separated by only 1.81 Å. Upon Li insertion, the 16c sites are gradually filled and the 8a sites emptied, resulting in the anticipated end composition $[Li_6]_{16c}[Li_1Ti_5]_{16d}(O_{12})_{32e}$.

The electrochemical Li insertion resulting in the gradual replacement of the 8a occupation by 16c occupation takes place with a very constant potential over a large range of overall Li concentrations, $0.1 < x < 2.9$. Such a voltage plateau is generally attributed to a two-phase coexistence of a Li-poor phase and a Li-rich phase during insertion.[4,6,7] Although during insertion this picture is correct, it has recently been demonstrated that in micrometer-sized $Li_{4+x}Ti_5O_{12}$ this true two-phase separation is unstable above 80 K[8] and domains of 16c occupation and 8a occupation intimately mix at a nanometer length scale,[9] which appears as a solid solution for diffraction.[8] This structural relaxation is accompanied by a small change in open circuit potential occurring in the course of hours.[8] The structural

[†] Department of Radiation, Radionuclides and Reactors, Faculty of Applied Sciences, Delft University of Technology.

[‡] Forschungszentrum Jülich GmbH.

[§] Delft Chem Tech, Faculty of Applied Sciences, Delft University of Technology.

(1) Dechanvres, A.; Raveau, B.; Sekkal, Z. *Mater. Res. Bull.* **1971**, *6*, 699–704.
(2) Johnston, D. C.; Prakash, H.; Zacharia, Wh.; Viswanat, R. *Mater. Res. Bull.* **1973**, *8*, 777–784.
(3) Ferg, E.; Gummow, R. J.; Dekock, A.; Thackeray, M. M. *J. Electrochem. Soc.* **1994**, *141*, L147–L150.
(4) Scharner, S.; Weppner, W.; Schmid-Beurmann, P. *J. Electrochem. Soc.* **1999**, *146*, 857–861.
(5) Wagemaker, M.; Van Der Ven, A.; Morgan, D.; Ceder, G.; Mulder, F. M.; Kearley, G. J. *Chem. Phys.* **2005**, *317*, 130–136.
(6) Murphy, D. W.; Cava, R. J.; Zahurak, S. M.; Santoro, A. *Solid State Ionics* **1983**, *9−10*, 413–417.
(7) Colbow, K. M.; Dahn, J. R.; Haering, R. R. *J. Power Sources* **1989**, *26*, 397–402.
(8) Wagemaker, M.; Simon, D. R.; Kelder, E. M.; Schoonman, J.; Ringpfeil, C.; Haake, U.; Lützenkirchen-Hecht, D.; Frahm, R.; Mulder, F. M. *Adv. Mater.* **2006**, *18*, 3169–3173.
(9) Wagemaker, M.; van Eck, E. R. H.; Kentgens, A. P. M.; Mulder, F. M. *J. Phys. Chem. B* **2009**, *113*, 224–230.

 10.1021/ja902423e © **2009 American Chemical Society**

relaxation may be rationalized by the zero-strain property causing the interface and strain energy due to the coexisting phases to be very low, which facilitates mixing of the two phases on a small length scale, in this case leading to a solid solution electrochemical response at relatively low temperatures (at room temperature or above 80 K).

Recent research has focused on nanosizing of electrode materials holding the promise of larger (dis)charge rates because it reduces the rate-limiting diffusion pathway in the electrode material. Interestingly, size-dependent studies on, e.g., TiO_2 anatase,[10] $LiFePO_4$,[11] and TiO_2 rutile,[12] have revealed strong differences in intrinsic material properties upon nanosizing. In some cases compositions inaccessible in the bulk materials were found, leading to larger Li capacities, and in all cases changing solubility limits upon nanosizing are observed, indicating fundamental changes in the thermodynamics of the nanosized compounds. These thermodynamic changes are currently related to strain[13] and interface and surface energy contributions that occur upon Li insertion.[10,14,15] In this context the zero-strain property of LTO is very interesting as it offers the possibility to study these nanosize effects in the absence of strain and interface energy. As demonstrated by the intimate mixing of the two end members of $Li_{4+x}Ti_5O_{12}$ in equilibrium at room temperature,[8,9] the energy penalty associated with coherent boundaries between the two end members is very low. This would imply that the reduction of the miscibility gap, and the reduction of the length of the voltage profile, due to strain and interface energy is absent in $Li_{4+x}Ti_5O_{12}$, making this material an important model system for the effects of nanoscaling.

Particle size dependent electrochemical properties of the LTO spinel were systematically investigated by Kavan et al.[16] Using LTO particles ranging from 1 μm to 9 nm in thin electrode films, they found an optimum battery performance for particles with a size around 20 nm ($\sim$100 m^2/g) at a voltage interval of 2.5−0.9 V. A recent electrochemical study revealed stable compositions of the microscale spinel beyond the $Li_7Ti_5O_{12}$ composition if the applied voltage interval included potentials as low as 0.01 V.[17] In $Li_7Ti_5O_{12}$ all octahedral 16c positions are filled; hence, additional Li will most likely reside in the unoccupied tetrahedral 8a positions, which are energetically unfavorable due to the short Li−Li distances and therefore require lower applied potentials. Ab initio calculations predict that this should lead to a distortion of the TiO_6 octahedra and a small increase (0.4%) of the unit cell volume for the composition $Li_{8.5}Ti_5O_{12}$.[18]

Here we study Li storage in nanosized LTO using neutron diffraction in addition to electrochemical (dis)charging, aiming at the direct observation of Li ions in the host structure and correlating the structural changes upon nanosizing with (dis)charge properties. This has led to a consistent picture revealing the impact of nanosizing LTO both on the structure and on the electrochemical characteristics including new insight into the origin of the curved voltage profile for nanoinsertion materials and an explanation of the optimal LTO particle size with respect to Li ion battery performance.

Methods

Synthesis. Microcrystalline $Li_4Ti_5O_{12}$ (99%) was obtained from Hohsen, and nanocrystalline $Li_4Ti_5O_{12}$ (99%) was provided by Altair Nano. The primary powder particle sizes of the nanoscale samples were obtained with transmission electron microscopy (TEM) by statistically averaging over 100 observed single particles, resulting in particle diameters of 31 ± 3 and 12 ± 2 nm; see Figure 2a. The crystalline purity of these samples was verified by X-ray diffraction (angles $10° < 2\theta < 80°$). Additionally, the atomic purity was verified with energy-dispersive spectroscopy (EDS). The chemically lithiated $Li_{4+x}Ti_5O_{12}$ samples were prepared by first mixing the $Li_4Ti_5O_{12}$ powder with hexane (anhydrous 95+%, Aldrich), after which *n*-butyllithium (1.6 M, Aldrich)[19] was added slowly while the mixture was stirred. The insertion is established in a potentiostatic way, where *n*-butyllithium has a potentiostatic driving force of 0.9 V versus Li^+/Li^0. To avoid lithium reacting with air and moisture, when respectively Li_2O and LiOH are formed,[20] two precautions have been taken. First, all powders have been dried in a vacuum oven at $\sim$400 K for several days to ensure water-free pristine materials. Second, the Li insertion has been performed in a glovebox under an argon atmosphere having less than 1 ppm oxygen or moisture. After preparation the samples were subjected to wet-chemical inductively coupled plasma spectroscopy (ICP) analysis to check the overall composition (ratio Li:Ti). These results confirmed the overall compositions as mentioned. Properties of the obtained samples are found in Table 1.

Electrochemistry. Electrochemical lithiation was carried out using a CR2320-type coin cell (Li/$LiPF_6$, 1 M (EC:DMC = 1:2)/LTO). Electrodes of LTO/carbon black/PVDF (80:10:10 wt %) have been prepared using a copper strip as the current collector. Galvanostatic discharge/charge curves were obtained using a current of 17.5 (mA h)/g (*C*/10).

Neutron Diffraction (ND). ND measurements were performed at the GEM diffractometer at ISIS (Rutherford Appleton Laboratory, U.K.). All samples were measured at room temperature in airtight cylindrical vanadium sample cans filled under a dry argon atmosphere. The resulting neutron diffraction spectra recorded at several banks (91.3°, 154.4°, and 63.9°) were simultaneously refined using the Rietveld method as implemented in GSAS.[21] The *d* spacing under consideration ranged from 0.3 to 4 Å. Besides the atomic and lattice parameters, the absorption and line-broadening parameters, crystal phase fractions, and background were fitted. The particle size broadening of the neutron diffraction reflections, see Figure 2b−d, confirmed the crystallite particle sizes as determined by TEM.

Results

Electrochemical (Dis)charging. Figure 1b shows the results of the galvanostatic (dis)charging at a *C*/10 rate down to 0.9 V (i.e., comparable to the potential at which the neutron diffraction samples have been intercalated in butyllithium) vs Li/Li^+ for the two crystal particle sizes. During the first discharge the well-established voltage plateau (region B) is observed around 1.55

(10) Wagemaker, M.; Borghols, W. J. H.; Mulder, F. M. *J. Am. Chem. Soc.* **2007**, *129*, 4323.
(11) Meethong, N.; Huang, H. Y. S.; Carter, W. C.; Chiang, Y. M. *Electrochem. Solid State Lett.* **2007**, *10*, A134–A138.
(12) Borghols, W. J. H.; Wagemaker, M.; Lafont, U.; Kelder, E. M.; Mulder, F. M. *Chem. Mater.* **2008**, *20*, 2949–2955.
(13) Meethong, N.; Huang, H. Y. S.; Speakman, S. A.; Carter, W. C.; Chiang, Y. M. *Adv. Funct. Mater.* **2007**, *17*, 1115–1123.
(14) Van der Ven, A.; Wagemaker, M. *Electrochem. Commun.* **2009**, *11*, 881–884.
(15) Wagemaker, M.; Mulder, F. M.; van der Ven, A. *Adv. Mater.* **2009**, *21*, 1–7.
(16) Kavan, L.; Prochazka, J.; Spitler, T. M.; Kalbac, M.; Zukalova, M. T.; Drezen, T.; Gratzel, M. *J. Electrochem. Soc.* **2003**, *150*, A1000–A1007.
(17) Ge, H.; Li, N.; Li, D. Y.; Dai, C. S.; Wang, D. L. *Electrochem. Commun.* **2008**, *10*, 719–722.
(18) Zhong, Z. Y.; Ouyang, C. Y.; Shi, S. Q.; Lei, M. S. *ChemPhysChem* **2008**, *9*, 2104–2108.
(19) (a) Thackeray, M. M.; David, W. I. F.; Goodenough, J. B. *Mater. Res. Bull.* **1982**, *17*, 785. (b) Whittingham, M. S.; Dines, M. B. *J. Electrochem. Soc.* **1977**, *124*, 1387–1388.
(20) Södergren, S.; Siegbahn, H.; Rensmo, H.; Lindström, H.; Hagfeldt, A.; Lindquist, S.-E. *J. Phys. Chem. B* **1997**, *101*, 3087.
(21) Larson, A. C. *GSAS*, Los Alamos National Laboratory, 1994.

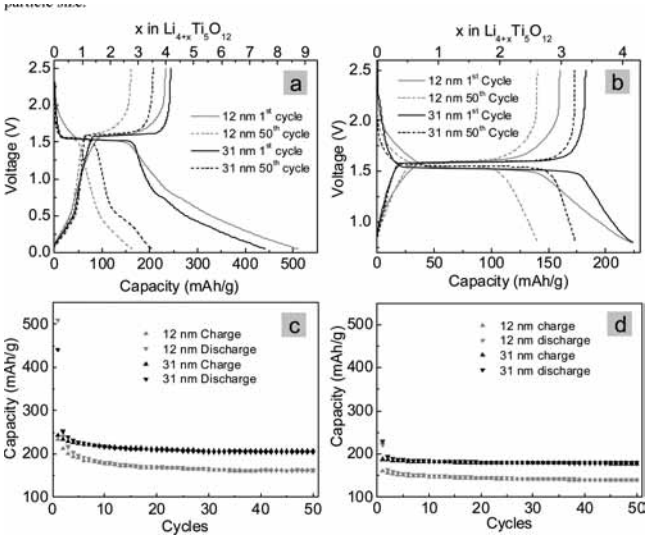

Figure 1. First galvanostatic and fiftieth discharge/charge for both 12 and 31 nm $Li_{4+x}Ti_5O_{12}$ crystallites at charge rate *C*/10 (17.5 (mA h)/g) (a) between 2.5 and 0.05 V vs Li/Li^+ and (b) between 2.5 and 0.9 V vs Li/Li^+. Capacity retention upon cycling for both 12 and 31 nm $Li_{4+x}Ti_5O_{12}$ crystallites at charge rate *C*/10 (c) between 2.5 and 0.05 V and (d) between 2.5 and 0.9 V.

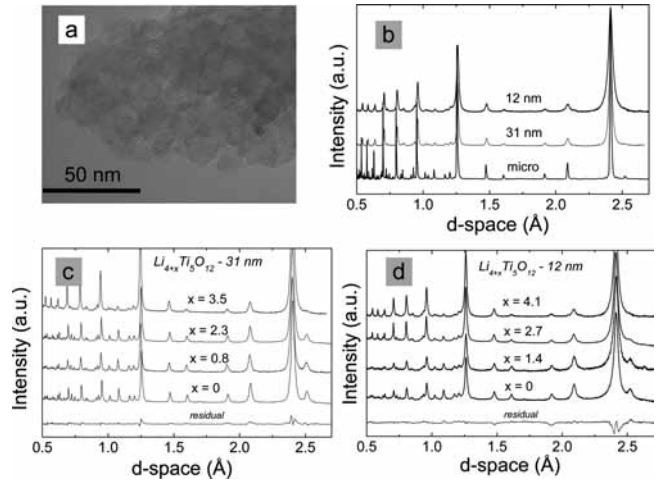

Figure 2. (a) TEM micrograph of 12 nm $Li_4Ti_5O_{12}$ crystallites. (b) Neutron diffraction patterns for microsized and 31 and 12 nm samples, with the maximal Li composition depending on the particle size: microsized, $Li_7Ti_5O_{12}$; 31 nm, $Li_{7.5}Ti_5O_{12}$; 12 nm, $Li_{8.1}Ti_5O_{12}$. (c) Neutron diffraction patterns for 31 nm $Li_{4+x}Ti_5O_{12}$ at several compositions *x*. (d) Neutron diffraction patterns for 12 nm $Li_{4+x}Ti_5O_{12}$ at several compositions *x*. The residuals shown are for $x = 0$ and are representative for all spectra.

V, representing the coexistence of Li 8a domains (Li occupies tetrahedral sites) with Li 16c domains (Li occupies octahedral sites).[4,7] For the smaller particle size, 12 nm, a much smaller capacity is discharged at a constant voltage; i.e., the plateau region is much smaller. Similar observations were made in other nanosized Li ion battery materials[11,22,23] and are related to changes in solubility limits due to strain and interface energy.[13,15]

Discharging to 0.05 V vs Li/Li^+, shown in Figure 1a, leads to a much larger capacity occurring mainly at voltages below 1.0 V and the largest for the smaller particle size (more than 500 (mA h)/g for 12 nm). A large part of this additional capacity (below 1.0 V) appears not reversible during the first subsequent charge. For a small part the extra capacity during the first cycle can be explained by Li intercalation in the 10 wt % carbon black present in the electrode. Assuming the capacity of carbon black to be 186 (mA h)/g (LiC_{12}), this accounts for only 20 (mA h)/g and is most likely observed as the small shoulder in Figure 1a around 0.75 V. In addition, the large capacity loss might be caused by irreversible reactions at the surface, such as the formation of a solid electrolyte interface (SEI) composed of organic lithium alkylcarbonates.[24] Although these mechanisms may explain the large irreversible capacity in the low-voltage region, they do not directly explain the capacity loss in the plateau region, clearly visible in the 50th discharge shown in Figure 1a and also seen when the discharge voltage is limited to 0.9 V in Figure 1b.

For discharging down to both 0.05 and 0.9 V the 12 nm particle size leads to a larger capacity during the first cycles; however, it surprisingly drops below the capacity of the 31 nm particles upon further cycling. This is mainly due to the capacity loss in the plateau region observed in Figure 1a,b, which is larger for the smaller particle size. The fact that this occurs for discharging down to both 0.05 and 0.9 V indicates that it is most likely not related to side reactions and the formation of the SEI. Hence, we conclude that the cycle performance represented by the (dis)charge capacity in the plateau region, is worse for the smaller particle size.

Interestingly, cycling down to 0.05 V as shown in Figure 1a leads for the 31 nm particle size to a reversible capacity of ~210 (mA h)/g, i.e., 20% larger compared to the theoretical capacity of 175 (mA h)/g when all 16c sites are occupied. (Note that this extra reversible capacity occurring below the constant-voltage plateau also compensates for the capacity loss in the constant-voltage region.) Ge et al. reported a comparable enhanced reversible capacity when cycled down to 0.01 V for LTO particle sizes that appear larger than presented here (the particle size was not reported, but judging from the voltage profiles, they are larger than those studied at present).[17] Apparently, LTO is able to host more Li when cycled to lower potentials.

Neutron Diffraction. Neutron diffraction was used to analyze chemically lithiated LTO materials to study the extra capacity that the nanomaterials are able to host as observed by electrochemical (dis)charging. Chemical lithiation was applied to produce large amounts of material (grams) as required for the neutron diffraction. Figure 2b shows the neutron diffraction patterns of the two nanosizes and the bulk material, all maximally chemically lithiated, clearly demonstrating the line width broadening due to the reduced particle size. Because *n*-butyllithium has a potentiostatic driving force of 0.9 V versus Li^+/Li^0, the Li capacity is expected to compare to the first electrochemical discharge presented in Figure 1b.

Detailed Rietveld refinement of the two particle sizes for a series of overall compositions, neutron diffraction patterns shown in Figure 2c,d, resulted in the oxygen positions in Figure 3b, the lattice parameters in Figure 3d, and the 8a and 16c site occupancies in Figure 3e. The very small change in unit cell volume upon lithiation in Figure 3d indicates that, similar to the micrometer-sized material, also the nanosized materials display the well-known zero-strain behavior. Whereas the maximum obtainable composition in microsized crystallites is

(22) Hu, Y. S.; Kienle, L.; Guo, Y. G.; Maier, J. *Adv. Mater.* **2006**, *18*, 1421.
(23) Sudant, G.; Baudrin, E.; Larcher, D.; Tarascon, J. M. *J. Mater. Chem.* **2005**, *15*, 1263–1269.
(24) Shu, J. *Electrochem. Solid State Lett.* **2008**, *11*, A238–A240.

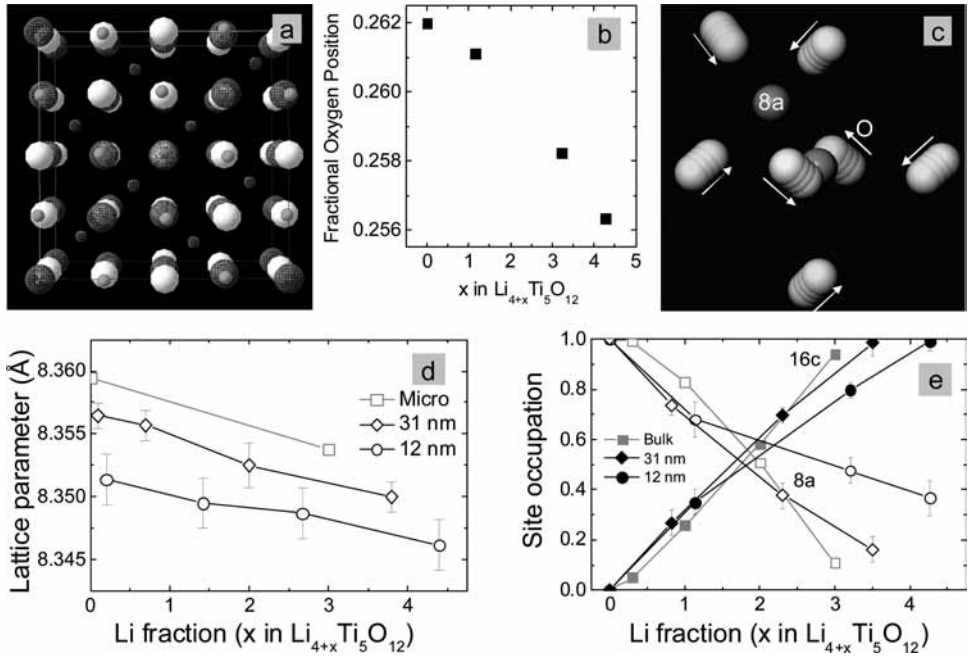

Figure 3. (a) Density difference Fourier map from the neutron diffraction data of the 12 nm $Li_{8.1}Ti_5O_{12}$ composition indicating partial 8a occupation in addition to full 16c occupation (wired contours) between the oxygen (white) and titanium (gray) spinel matrix. (b) Oxygen position in 12 nm $Li_{4+x}Ti_5O_{12}$ as a function of the overall lithium composition. (c) Neighboring Li (gray) 8a and 16c sites with the surrounding oxygen tetrahedron and octahedron indicating decreasing tetrahedron and octahedron dimensions, leading to better screening of the repulsing Li ions. For demonstration purposes the oxygen shift has been amplified by a factor of 2. (d) Lattice parameters and (e) fractional Li occupation in both 8a (open symbols) and 16c (closed symbols) sites of micrometer and 31 and 12 nm sized $Li_{4+x}Ti_5O_{12}$ as a function of the overall lithium composition.

Table 1. Li Composition in $Li_{4+x}Ti_5O_{12}$ As Determined with Galvanostatic (First) Discharge and ICP and Neutron Diffraction on Chemically Lithiated Materials

Li fraction	first discharge to 0.9 V	first discharge to 0.05 V [capacity (mA h)/g]	chemical lithiation, neutron diffraction	chemical lithiation, ICP
12 nm	$Li_{7.84}Ti_5O_{12}$	$Li_{12.8}Ti_5O_{12}$ [512]	$Li_{8.1}Ti_5O_{12}$	$Li_{8.4}Ti_5O_{12}$
31 nm	$Li_{7.45}Ti_5O_{12}$	$Li_{11.6}Ti_5O_{12}$ [442]	$Li_{7.5}Ti_5O_{12}$	$Li_{7.8}Ti_5O_{12}$

$Li_7Ti_5O_{12}$ (16c sites almost fully occupied), the Li occupancy of the tetrahedral (8a) and octahedral (16c) sites as a function of the overall composition in the 31 and 12 nm materials leads to significantly higher capacities of $Li_{7.5}Ti_5O_{12}$ and $Li_{8.1}Ti_5O_{12}$, respectively. The fit results in Figure 3e indicate that in both maximally lithiated nanosized samples the 16c site is almost completely occupied, which is not the case in bulk LTO. More remarkable is that additionally the 8a site is partially occupied by a 0.17 fraction in the 31 nm crystallites and even a 0.37 fraction in the 12 nm crystallites. This is also demonstrated by the density difference Fourier map for the $Li_{8.1}Ti_5O_{12}$ composition in Figure 3a, resulting from a comparison of the actual neutron diffraction data with a fit having no Li ions included. In this way the density difference plot of the atomic density indicates the missing Li ion density in the model. In combination with the fit results, this indicates that in addition to the fully occupied 16c site part of the 8a site is occupied, hence indicating simultaneous occupation of both sites in at least part of the material. The change of the fractional oxygen position upon lithiation beyond the $Li_7Ti_5O_{12}$ composition (16c fully occupied) is most likely a consequence of the increasing simultaneous 8a and 16c occupation in part of the material. The change in the oxygen position and its impact on the tetrahedral Li 8a site and octahedral Li 16c site are shown in Figure 3b. A quantitative comparison between the maximum capacity by electrochemistry, diffraction, and ICP is presented in Table 1. All three techniques show that the maximum lithium fraction increases as the particle size decreases. The slightly larger capacities obtained by ICP most likely reflect the fact that ICP detects all Li species, possibly also Li atoms bound at the surface. The larger capacity found by neutron diffraction and ICP compared to the capacity in the first discharge down to 0.90 V may indicate that the chemical reaction with BuLi effectively appears at a lower potential versus Li/Li^+ in these nanosamples. A rationale for such lower potential might be that butyllithium in the nanomaterials finds a relatively more favorable reaction for a large part of the butyllithium added due to an exchange reaction of Li with surface-bound H, the latter always present at oxide surfaces.

The particle sizes of both pristine nanosized samples were determined by examination of the line width broadening from the neutron diffraction data and appeared in close agreement with the direct observation in the TEM micrographs. However, comparing the fit results on the lithiated LTO samples and the pristine samples shows a small, but significant decrease in particle size of about 1−2 nm, irrespective of the overall particle size. This can indicate that the Li insertion process leads to a change in the surface structure of the particle or mechanical failure of a surface layer of the particles.

Discussion

Increased Capacity Nanoparticles (2.5−0.9 V). Recently, Ge et al. demonstrated that bulk spinel $Li_{4+x}Ti_5O_{12}$ discharged down to 0.01 V leads to a higher reversible capacity[17] compared to discharge down to approximately 0.9 V vs Li/Li^+, the latter

leading to the well-established composition $Li_7Ti_5O_{12}$ (175 (mA h)/g) where the octahedral (16c) sites are occupied by Li ions and the tetrahedral (8a) sites are empty. This indicates that in the 0.9−0.01 V window additional Li ions can be inserted into the less favorable sites that are available in the lithiated LTO host. Such additional occupancy was recently suggested by first-principle calculations to occur when discharged down to 0.05 V vs Li/Li^+, leading to only 0.4% volume expansion up to composition $Li_{8.5}Ti_5O_{12}$.[18] The additional Li was predicted to occupy the 8a sites,[18] leading to short 8a−16c Li distances that are energetically unfavorable, explaining the lower insertion voltage.[5]

The present neutron diffraction results and ICP analysis of chemically lithiated materials prove that LTO can host additional Li, a consequence of the additional 8a site occupancy next to the fully occupied 16c sites. However, the chemical lithiation implies that the additional insertion occurs at a voltage around 0.9 V vs Li/Li^+, which is much higher than the 0.01 V discharge voltage used by Ge et al.[17] and the 0.05 V indicated by the ab initio calculations.[18] The essential difference between the materials considered at present and by Ge et al. is that the presently studied materials are nanosized, which apparently leads to the same enhanced capacity as micrometer-sized materials, but at more favorable higher discharge voltages. The results in Table 1 and Figure 3e prove that reducing the particle size, at the same insertion potential, enhances the capacity due to the increasing 8a occupancy. Realizing that diffraction is a bulk technique (it probes the average occupancies) and that the far majority of the atoms in the particle sizes studied (12 and 31 nm) reside in the bulk (not at the surface), it appears that nanosizing has a global impact on the properties of these particles. Nevertheless, it may well be, and in fact is very likely, that at the near-surface region 8a occupancies may reach relatively larger values. The expected diffusion pathway in these spinel materials is 16c−8a−16c;[25] hence, Li occupying 8a sites in addition to 16c sites will hinder the diffusion considerably. Therefore, it is reasonable to assume that the 8a occupancy, responsible for the increased capacity, is higher at near-surface regions (due to shorter diffusion distances). Further, the energetically unfavorable short 8a−16c Li distances are likely to cause the local structure to deform, which may be expected to be easier at the near-surface region. Clearly, for smaller particle sizes the surface region represents a larger fraction of the particle volume, and hence, high 8a occupancy in the near surface region would explain the higher average 8a occupancy in smaller particle sizes as observed in Figure 3e and Table 1. These observations are in line with observed increased capacity in lithiated anatase and rutile TiO_2 nanoparticles, where the shorter average diffusion distance enables higher Li occupancies at near-surface regions, which represent a significantly larger fraction of the material for a smaller particle size.[10,12,26]

Increased Capacity Nanoparticles (2.5−0.05 V). Galvanostatic discharge in the nanomaterials down to 0.05 V vs Li/Li^+ leads to even much larger capacities well above $Li_9Ti_5O_{12}$, which would imply a Ti valence below Ti^{3+}; see Table 1. This additional capacity appears to scale with the particle specific surface area and may at first instance be subscribed to irreversible reactions at the surface, such as the formation of organic lithium alkylcarbonates,[24] since most of the capacity below 0.9 V appears to be lost at the first charge. However, there still is a significant amount of reversible capacity present below 0.9 V. Most likely this is due to more simultaneous 8a and 16c occupation and due to capacitively stored Li ions at the surface. The simultaneous 8a and 16c occupation at the surface will hinder further Li insertion, leading to large polarization below the open cell potential.

Curved Voltage Profile. Similar to other nanosized Li ion host materials undergoing a first-order phase transition, such as $LiFePO_4$[11] and anatase TiO_2,[23] nanosized spinel $Li_{4+x}Ti_5O_{12}$ also displays a curved voltage profile reducing the length of the constant voltage plateau as observed in Figure 1b. Recent research has indicated that the reduced voltage plateau may be a consequence of a reduction of the miscibility gap.[11,27] A rationale is found in the relatively large impact of strain[13] and/or interface energy[15] in nanomaterials as a result of the coherent interface existing between the Li-poor and Li-rich phases. Strain will occur due to a difference in the unit cell volume of both coexisting phases, and interface strain is similar to the surface energy (tension) of the local deviation of the regular atomic positions near the interface between the two phases. Both strain and interface energy cause an energy penalty that may be expected to become relatively large in smaller particles because the amount of atoms near the interface will be relatively larger in small particles. This energy penalty effectively lowers the gain in energy by forming a two-phase system (in $Li_{4+x}Ti_5O_{12}$ this would be $Li_{4+\alpha}Ti_5O_{12}$ and $Li_{7-\beta}Ti_5O_{12}$) rather than a solid solution, effectively extending the solubility limits of both end members (α and β become larger). Consequently, the voltage plateau, representing the two-phase coexistence, will be present in a smaller composition domain. In this context the voltage curves from nanosized spinel $Li_{4+x}Ti_5O_{12}$ are of fundamental interest because $Li_{4+x}Ti_5O_{12}$ is well-known to be a "zero-strain material", the consequence of both end members ($Li_4Ti_5O_{12}$ and $Li_7Ti_5O_{12}$) having barely indistinguishable unit cell volumes. Since the structures are so similar, both strain and interface energy due to coherent phase boundaries can be expected to be very small. This is compellingly demonstrated by the solid solution behavior of microsized $Li_{4+x}Ti_5O_{12}$, which in equilibrium at room temperature forms a mixture of nanodomains of the two end members,[8,9] indicating that the coherent interface between the two end members does not raise a significant energy barrier. Therefore, the observed reduction of the voltage plateau upon downsizing the $Li_{4+x}Ti_5O_{12}$ particles observed in Figure 1b must have another origin than strain and/or interface energy. To explain this, we propose that the curved voltage region above 1.55 V at low compositions and below 1.55 V at high compositions is due to a different environment experienced by Li ions residing near the surface of the particles compared to those in the bulk. This is in line with the discussed energetically unfavorable 8a−16c Li ion neighbors, which appear to be possible at relatively high voltages in the near-surface environment, indicating a different structural environment in the unit cells located in the vicinity of the surface. Also ab initio calculations on $LiFePO_4$ support this suggestion, because the

(25) Verhoeven, V. W. J.; de Schepper, I. M.; Nachtegaal, G.; Kentgens, A. P. M.; Kelder, E. M.; Schoonman, J.; Mulder, F. M. *Phys. Rev. Lett.* **2001**, *86*, 4314–4317.

(26) (a) Wagemaker, M.; Lutzenkirchen-Hecht, D.; van Well, A. A.; Frahm, R. *J. Phys. Chem. B* **2004**, *108*, 12456–12464. (b) Borghols, W. J. H.; Lutzenkirchen-Hecht, D.; Haake, U.; van Eck, E. R. H.; Mulder, F. M.; Wagemaker, M. *Phys. Chem. Chem. Phys.* **2009**, *11*, 5742–5748.

(27) Kobayashi, G.; Nishimura, S. I.; Park, M. S.; Kanno, R.; Yashima, M.; Ida, T.; Yamada, A. *Adv. Funct. Mater.* **2009**, *19*, 395–403.

redox potential appears to depend strongly on the orientation of the surface plane, redox potentials both above and below the bulk redox potential occurring.[28] Although the referred study only considers surface sites, it appears very plausible that the environment in the unit cells near the surface is also different from that of the bulk, leading to a distribution of redox potentials that approaches the bulk value further into the bulk of the particle. For smaller particles relatively more Li ions reside in the near-surface area, and therefore, the distribution of redox potentials contributes a relatively larger capacity, leading to the curved voltage profile. This leads to the following picture of the Li insertion in spinel $Li_{4+x}Ti_5O_{12}$: Initial lithiation leads to occupation of 16c sites near the surface, being energetically more favorable, hence occurring at higher voltages. Further lithiation leads to occupation of the "bulk" sites in the nanoparticles. Before the $Li_7Ti_5O_{12}$ composition (all 16c sites occupied) is reached, the low-voltage 16c sites are filled. Even further lithiation leads to additional 8a occupation (energetically less favorable) next to the completely filled 16c occupied sites in the near-surface region, leading to a size-dependent overall Li composition reaching overall composition $Li_{8.1}Ti_5O_{12}$ in 12 nm particles.

Irreversible Capacity Loss. In a systematic particle size dependent study, Kavan et al. concluded that reducing the LTO particle size leads to a systematic decrease of the Li diffusion coefficient, compensated by the large surface area, leading to an optimal particle size between 130 and 20 nm depending on the charge rate.[16] An increasing capacity loss with decreasing particle size was observed and explained by the decreasing diffusion coefficient. Consideration of Figure 1c,d reveals that after a few cycles the 12 nm particles show a larger capacity loss than for the 31 nm particles, consistent with the results of Kavan et al. Investigation of Figure 1a,b shows that the capacity loss for both particle sizes is mainly in the plateau region. Polarization effects due to SEI formation could explain a more sloped voltage plateau, effectively leading to a reduction of the plateau, which may be expected to have a larger impact on the smaller particle size having a larger particle surface. However, if polarization were the explanation, a large difference between the charge and discharge voltages would be observed,which, as can be seen in Figure 1a,b, is not the case. Also, if the SEI were responsible for the polarization, it would be expected to disappear largely when the potential window is restricted to 2.5−0.9 V rather than 2.5−0.05 V. Comparison of parts a and b and parts c and d of Figure 1 indicates almost the same capacity loss for both voltage windows. Therefore, we conclude that reversible capacity is lost in the plateau region, and this capacity loss is larger for the smaller particle size. The capacity loss in the plateau region must indicate that there is less Ti^{4+} to be reduced in the LTO structure after the first few cycles. Because the capacity loss scales with the particle surface area, we suggest two possible origins related to the particle surface: (1) irreversibly bonded Li ion capacity at the near-surface area of the particles and (2) mechanical failure of a thin surface layer. The lattice parameters in Figure 3d show that there appears to be no reason to assume mechanical failure up to overall composition $Li_{8.1}Ti_5O_{12}$. However, this is an average composition, and as already discussed, the Li ion concentration in the near-surface region may be expected to be larger. Ab initio calculations indicate that above composition $Li_{8.5}Ti_5O_{12}$ one may expect much larger structural changes.[18] Therefore, these large distortions may lead to surface reconstruction locally at the surface, an effect which appears to be possible in transition-metal oxides.[29] Alternatively, larger structural changes may lead to mechanical failure (HRTEM was attempted on these lithiated materials, but failed most likely due to the instability of the particle surface under the beam). In particular, if the simultaneous occupation of 16c and 8a sites locally at the surface leads to compositions above $Li_9Ti_5O_{12}$, this would imply a Ti valence below 3+, which may lead to mechanical failure of a thin surface layer. Diffraction indicates that the (chemical) lithiation leads to slight broadening of the reflections, indicating a reduced crystallite size and/or increased tension, indicating indeed one of the two mechanisms proposed. Both processes appear to effectively passivate the near-surface area, which, assuming a constant layer thickness of the passivated surface layer, explains why the irreversible capacity in the plateau region is larger for smaller particles. Also, the low amount of vacancies due to the simultaneous occupation of 16c and 8a sites in smaller particles, mostly due to the surface region that represents a larger fraction of the particle in a smaller particle, can be expected to lead to a reduction of the diffusion coefficient, explaining the observations by Kavan et al.[16] Additionally, some irreversible capacity loss of Li at the surface of transition-metal oxides may result, when the oxygen-terminated surface, which is richly decorated by H_2O/OH groups, exchanges H for Li while protonating the electrolyte. At the potentials used the resulting Li_2O-like surface layer will not easily give up its Li during electrochemical charge, adding to the irreversibility. In amorphous TiO_2 such lithium appears to be bound to the surface oxygen, modifying the surface structure and effectively reducing the oxygen coordination of Ti.[30]

Concluding Remarks

Neutron diffraction proves increased Li ion capacity in nanosized spinel $Li_{4+x}Ti_5O_{12}$ due to simultaneos occupation of both tetrahedral (8a) and octahedral (16c) sites, which may be expected to be energetically unfavorable due to the short distance between these sites. The fact that smaller particle sizes lead to larger capacities suggests that the simultaneous 8a and 16c occupation is more easily accommodated in the near-surface region of the particle compared to the bulk, explaining the relatively high (dis)charge voltages at which it takes place. The curved shape of the voltage curve and the consequently decreasing constant-voltage plateau region of nanosized $Li_{4+x}Ti_5O_{12}$ are very similar to those of other nanosized compounds, such as $LiFePO_4$, displaying a first-order phase transition. These voltage profiles, typical for nanoparticles, have recently been explained to be the consequence of strain and/or interface energy, which has relatively more impact in smaller particles. However, the unique property of spinel $Li_{4+x}Ti_5O_{12}$ is that both strain and interface energy are practically absent in $Li_{4+x}Ti_5O_{12}$ due to the similar structures and lattice parameters of both end members. This indicates another source of the curved voltage profile in $Li_{4+x}Ti_5O_{12}$, which we argue to be a distribution of different redox potentials at the near-surface region of the particle, which will represent a larger part of the total capacity for smaller particles, explaining the reduced voltage profile. We emphasize that this surface effect is likely to play an important role in nanosized intercalation compounds

(28) Wang, L.; Zhou, F.; Meng, Y. S.; Ceder, G. *Phys. Rev. B* **2007**, *76*, 16.

(29) Erdman, N.; Poeppelmeier, K. R.; Asta, M.; Warschkow, O.; Ellis, D. E.; Marks, L. D. *Nature* **2002**, *419*, 55–58.

(30) Borghols, W. J. H.; Lutzenkirchen-Hecht, D., Haake, U.; Chan, W.; Lafont, U.; Kelder, E. M.; van Eck, E. R. H.; Mulder, F. M.; Wagemaker, M. Manuscript in preparation 2009.

in general. Consistent with previous studies, decreasing the particle size leads to a larger irreversible capacity, which mostly appears in the plateau region. The high Li site occupations observed in neutron diffraction explain the previously reported decrease of the diffusion coefficient with decreasing particle size. The apparent decrease of the particle size suggests passivation of the surface region due to irreversible surface reconstruction and/or mechanical failure. Hence, the irreversible capacity will be larger for smaller particles having a larger surface area.. As a result we conclude that, in terms of the capacity, an optimum particle size exists depending on the voltage window.

Acknowledgment. This work is a contribution from the Delft Institute for Sustainable Energy (DISE). Financial support from The Netherlands Organization for Scientific Research (NWO) is acknowledged for both beam time at ISIS (U.K.) and the CW-VIDI grant of M.W. We thank Winfried Kockelmann for assistance with the neutron diffraction measurements at GEM (ISIS). We thank the Alistore network for providing access to TEM measurements and the electrochemical laboratories.

JA902423E